crystals

MDPI

Article

Regium Bonds between Silver(I) Pyrazolates Dinuclear Complexes and Lewis Bases (N_2, OH_2, NCH, SH_2, NH_3, PH_3, CO and CNH)

Ibon Alkorta [1,*], Cristina Trujillo [2], Goar Sánchez-Sanz [3,4] and José Elguero [1]

1 Instituto de Química Médica, CSIC, Juan de la Cierva, 3, E-28006 Madrid, Spain; iqmbe@iqm.csic.es
2 School of Chemistry, Trinity Biomedical Sciences Institute, Trinity College, Dublin, 152–160 Pearse St, Dublin 2, Ireland; trujillc@tcd.ie
3 Irish Centre of High-End Computing, Grand Canal Quay, Dublin 2, Ireland; goar.sanchez@ichec.ie
4 School of Chemistry, University College Dublin, Belfield, Dublin 4, Ireland
* Correspondence: ibon@iqm.csic.es

Received: 28 January 2020; Accepted: 19 February 2020; Published: 24 February 2020

Abstract: A theoretical study and Cambridge Structural Database (CSD) search of dinuclear Ag(I) pyrazolates interactions with Lewis bases were carried out and the effect of the substituents and ligands on the structure and on the aromaticity were analyzed. A relationship between the intramolecular Ag–Ag distance and stability was found in the unsubstituted system, which indicates a destabilization at longer distances compensated by ligands upon complexation. It was also observed that the asymmetrical interaction with phosphines as ligands increases the Ag–Ag distance. This increase is dramatically higher when two simultaneous PH_3 ligands are taken into account. The calculated ^{109}Ag chemical shielding shows variation up to 1200 ppm due to the complexation. Calculations showed that six-membered rings possessed non-aromatic character while pyrazole rings do not change their aromatic character significantly upon complexation.

Keywords: non-covalent interactions; regium bonds; silver(I); coinage metals; pyrazolates; phosphines

1. Introduction

Non-covalent interactions (NCIs) are present in complexes formed between two or more Lewis acids and Lewis bases. In fact, those interactions are commonly named by the Lewis acid [1]. On the one hand, a Lewis base (LB) or a LB motif is associated with a region of space where there exists an excess of negative charge (i.e., electron density) in the proximity of an atom or atoms within a molecule. This is predominant in anions and in some neutral molecules such as those that exhibit lone pairs (LP: carbenes, amines, phosphines, N-oxides, etc.), multiple bonds (olefins, acetylenes, benzenes and other aromatic molecules), single bonds (alkanes, dihydrogen, etc.), radicals, metals (rarely), etc. On the other hand, a Lewis acid (LA) is associated with a region of space where there is an excess of positive charge (in other words a deficit of negative charge or electron deficiency) in the proximity of an atom or atoms in a molecule. This can be found in cations, molecules or atoms exhibiting σ- and π-holes and metals (frequently). The concept of a σ-hole was introduced by Politzer et al. [2–5] to describe regions of positive potential along the vector of a covalent bond. It was latter extended to other situations, for example, the π-hole [6–11] (positive electrostatic potential perpendicular to an atom of a molecular framework) and lone pair hole (similar to σ-hole but along the atom–lone pair direction) [12–14]. The maximum value of the molecular electrostatic potential within a given molecular density isosurface surface, $V_{S,max}$, has also been classified based on the nature of the orbitals (s-, p- and d- orbitals) and it is associated with the corresponding deficiencies (σ_s-, σ_p- and σ_d-holes) [15].

There is a wide variety of non-covalent interactions due to most groups of the periodic table being associated with a certain type of NCI: starting from the archetypical hydrogen bond (HB) there are "alkali bonds" (group 1) [16,17], "alkaline earth bonds" (group 2) [18–20], "regium bonds" (groups 10 and 11) [21–23], "triel bonds" (group 13) [24], "tetrel bonds" (group 14) [25–28], "pnictogen (also called pnicogen) bonds" (group 15) [29–31], "chalcogen bonds" (group 16) [32–35], "halogen bonds" (group 17) [36,37], and "aerogen bonds" (group 18) [38]. Regium (or coinage-metal bonds) bonds involve mainly coinage metals, Cu, Ag and Au. These weak interactions are particularly interesting since they are associated with organometallic chemistry. However, it is necessary to clearly differentiate between clusters (e.g., Au_2 or Ag_{11}) [22,39] and molecules (e.g., AuX) [40,41]. Recent published works show an increased interest in regium bonds, some example of which are discussed here [42–45].

In this article, the dinuclear silver(I) pyrazolates (Scheme 1) have been considered following a previous paper on trinuclear silver(I) pyrazolates [46]. The effect of the ligands on the silver atom and the substituents on the pyrazole rings on the structure, energetic, electronic and magnetic properties have been analyzed.

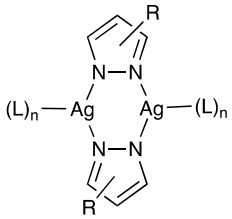

R = H, 4-NO_2, 3,5-diMe, 4-Cl,

L = N_2, OH_2, NCH, SH_2, NH_3, PH_3, CNH

n = 0, 1, 2, 4

$(PzAg)_2$	$(PzAg)_2(PH_3)_2$	$(4NO_2pzAg)_2(PH_3)$
$(PzAg)_2(N_2)_2$	$(PzAg)_2(CO)_2$	$(4NO_2pzAg)_2(PH_3)_2$
$(PzAg)_2(OH_2)_2$	$(PzAg)_2(CNH)_2$	$(4NO_2pzAg)_2(PH_3)_4$
$(PzAg)_2(NCH)_2$	$(PzAg)_2(PH_3)$	$(DMepzAg)_2$
$(PzAg)_2(SH_2)_2$	$(PzAg)_2(PH_3)_4$	$(4ClpzAg)_2$
$(PzAg)_2(NH_3)_2$	$(4NO_2pzAg)_2$	$(DMepzAg)_2(PH_3)_2$
		$(4ClpzAg)_2(PH_3)_2$

Scheme 1. General structure of the complexes under study and their corresponding names.

2. Materials and Methods

2.1. Cambridge Structural Database Search

The Cambridge Structural Database (CSD) [47] version 5.40 with updates from November 2018, May 2019, and August 2019 was searched for systems with cyclic $(Pz\text{-}Ag)_2$ structure. The geometrical characteristics of these systems have been analysed.

2.2. Ab Initio Calculations

The geometry of the systems have been fully optimized using the MP2 computational method [48–51] and the jul-cc-pVDZ basis set [52–54] for all the atoms except for the silver atoms, of which the aug-cc-pVDZ-PP effective core potential basis set [55] has been used. Frequency calculations have been carried out at the same computational level to verify that the obtained structures correspond to energetic minima. Dissociation energies have been obtained as the difference between the sum of the energies of the isolated monomers in their optimized geometry and the energy of the complex. These calculations have been carried out with the Gaussian-16 program [56].

The molecular electrostatic potential on the 0.001 au electron density isosurface (MESP) was calculated with the Gaussian16 program, analyzed with the Multiwfn program [57] and represented with the JMol program [58].

The topological analysis of the electron density was carried out by means of the quantum theory of atoms in molecules (QTAIM) method [59–62] using the AIMAll program [63]. This method identifies the points of space where the gradient of the electron density vanishes (critical points) and based on the number of positive curvatures characterizes them as nuclear attractors (3, −3), bond critical points (3, −1), ring critical points (3, +1) or cage critical points (3, +3). By connecting the bond critical points with the nuclear attractor, following the minimum gradient path, the molecular graph is obtained.

The natural bond orbital (NBO) method [64] was employed using the NBO-3 program to evaluate atomic charges, and to analyze charge-transfer interactions between occupied and unoccupied orbitals.

The TOPMOD program [65] has been used to analyze the areas of electron concentration in terms of the electron localization function (ELF) [66]. For the three-dimensional plots, a convenient ELF value of 0.7 was used [67].

Relativistic-corrected NMR chemical shielding values for the geometries optimized at MP2 level were obtained using the relativistic ZORA spin–orbit Hamiltonian [68,69], the BP86 functional [70–72], and the full electron QZ4P basis [73]. In addition, the nuclear-independent chemical shift (NICS) [74] at the centre and 1 Å above the centre of the ring formed by the two Ag atoms and the pyrazole moieties were calculated to study the aromaticity of all systems. In addition, a scan of the NICS values from 0 to 2 Å in steps of 0.25 Å for $(PzAg)_2$ was calculated [75,76]. These calculations have been performed with the ADF-2017 program [77].

3. Results and Discussion

In this paper we will report the study of nineteen compounds corresponding to the general formula depicted in Scheme 1 and named by a simple code that allows to easy identification: $(R\text{-}pzAg)_2(L)_n$. Firstly, the substituents (R) on the pyrazole ring are indicated: Pz, $4NO_2pz$, DMepz and 4Clpz for the unsubstituted (H), 4-nitro, 3,5-dimethyl, and 4-chloro derivatives, respectively. Secondly, the ligands (L) interacting with the silver atoms are indicated. Thus, for instance, $(4NO_2pzAg)_2(PH_3)_4$ corresponds to the (4-nitropyrazole:$Ag)_2$ cyclic structure with four phosphines interacting with the silver atoms (two phosphines per each silver atom).

3.1. CSD Search

A search in the Cambridge Structural Database has been carried out and the resulting compounds with the structure represented in Scheme 1 were summarized and reported in Table 1 ordered by increasing Ag–Ag intramolecular distance. Two simplified views of these structures can be found in Table S1 of the Supplementary Materials. Structures with dinuclear silver(I) pyrazolates without ligands were not found within the CSD search.

As observed by the crystallographic data, the Ag–Ag distance ranges between 4.305 Å (ZIGSEQ) and 3.392 Å (FINWOR). The shortest distances correspond to complexes with only two ligands present concomitantly with the 3,5-bis-CF_3 substituent on the pyrazole. It is also clear that the larger the number of ligands, the longer the intramolecular Ag–Ag distance. Moreover, it is noteworthy that, in structures with four phosphines ligands, the Ag–Ag distance increases as the substitutes of the pyrazole are H < 4-Cl < 4-NO_2. These results will be compared against our theoretical calculations in the following sections.

Concerning the conformation of the six-membered rings in the crystal structures (similar to those of 1,4-cyclo-hexadiene, 9,10-dihydroanthracenes, phenothiazines, etc.), very little energy differences between those conformations in the crystals were found, in agreement what was proposed by Rasika Dias [78]. Regarding the tetrahedral configuration of Ag(I) atom, we have used Houser's τ_4 index [79] as recommended by Raptis [80]. This index is defined as:

$$\tau_4 = [360 - (\alpha + \beta)]/141 \quad (1)$$

where, α and β correspond to the two largest angles of the six angles around the tetrahedral silver atom. The values of τ_4 range from 1 (perfect tetrahedral geometry, i.e., $\tau_4 = [360 - (109.5 + 109.5)]/141 = 1$) to 0 (perfect square planar geometry). The τ_4 values obtained for three substituents, 0.9 (RATFEX and ZIGSIU) are very similar to those for 4 substituents (ZIGROZ and ZIGSEQ, 0.89 and 0.88 respectively) with both identical Ag atoms. The two lowest values (0.78) correspond to a substituent that differs from PPh_3 (see notes (a) and (b) of Table 1).

Table 1. Results of the Cambridge Structural Database (CSD) search. Abbreviations: nature of the pyrazolate anion, nature of the ligand (L), number of ligands; Ag(I)–Ag(I) distance in Å, silver–ligand distance in Å, conformation of the six-membered ring and tetrahedral configuration of the Ag (τ_4 index).

Refcode	Pyrazolate	Ligand (L)	N° of Ls	Ag–Ag	Ag–L	Conformation	τ_4 index
FINWOR	3,5-bis-CF_3	3,5-bis-CF_3-pyrazole-Ag	2	3.392	2.250	Nearly planar	—
PIRCUR	3,5-bis-CF_3	PPh_3	2	3.425	2.343	Boat	—
PIRCUR	3,5-bis-CF_3	PPh_3	2	3.425	2.414	Boat	—
FINWIL	3,5-bis-CF_3	PPh_3	2	3.479	2.366	Twisted boat	—
IPIGOD	3,5-bis-CF_3	2,4,6-collidine	2	3.499	2.277	Boat + flattened chair	—
IPIGOD	3,5-bis-CF_3	2,4,6-collidine	2	3.499	2.254	Boat + lattened chair	—
IPIGOD	3,5-bis-CF_3	2,4,6-collidine	2	3.502	2.269	Boat + flattened chair	—
IPIGOD01	3,5-bis-CF_3	2,4,6-collidine	2	3.562	2.253	Half boat	—
IPIGOD01	3,5-bis-CF_3	2,4,6-collidine	2	3.562	2.253	Half boat	—
SOJCIG	3,5-bis-CF_3	3,5-bis-CF_3-pyrazole-Ag	2	3.632	3.218	Chair	—
SOJCIG	3,5-bis-CF_3	pyrazole-Ag	2	3.632	2.258	Chair	—
RATFEX	Parent	PPh_3	3	3.706	2.370	Flattened chair	0.90
RATFEX	Parent	PPh_3	3	3.706	2.484	Flattened chair	
RATFEX	Parent	PPh_3	3	3.706	2.461	Flattened chair	
ZIGRUF	4-Cl	PPh_3	3	3.707	2.374	Flattened boat	0.83
ZIGRUF	4-Cl	PPh_3	3	3.707	2.475	Flattened boat	
ZIGRUF	4-Cl	PPh_3	3	3.707	2.485	Flattened boat	
ZIGSIU	4-NO_2	PPh_3	3	3.827	2.379	Boat	0.90
ZIGSIU	4-NO_2	PPh_3	3	3.827	2.495	Boat	
ZIGSIU	4-NO_2	PPh_3	3	3.827	2.469	Boat	
RATFAT	Parent	PPh_3	2	3.870	2.376	Planar	—
KIRXIV	Parent	(a)	2 (4)	3.900	2.532	Planar	0.78
KIRXIV	Parent	PPh_3	4	3.900	2.539	Planar	
ZIGSAM	4-Cl	(b): PR_3	4	4.205	2.460	Twisted	0.78
ZIGSAM	4-Cl	PR_3		4.205	2.534	Twisted	
ZIGROZ	4-Cl	PPh_3	4	4.209	2.484	Twisted	0.89
ZIGROZ	4-Cl	PPh_3	4	4.209	2.500	Twisted	
ZIGSEQ	4-NO_2	PPh_3	4	4.305	2.502	Twisted	0.88
ZIGSEQ	4-NO_2	PPh_3	4	4.305	2.487	Twisted	
max	—	—		4.305	3.218	—	—
min	—	—		3.392	2.250	—	—

(a) Two P ligands that corresponds to four P atoms.

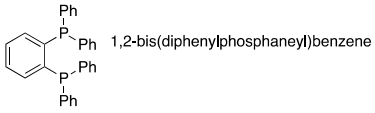

(b) A P ligand in an adamantane type molecule:

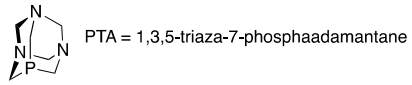

3.2. Electronic Properties of the Isolated $(PzAg)_2$ System

The isolated $(PzAg)_2$ system calculated at MP2 level presents a planar structure with D_{2h} symmetry, where the silver atoms are equidistant to the pyrazole rings with an intramolecular Ag–Ag distance of 2.801 Å (Table S2). This intramolecular distance is slightly larger than that of the Ag_2 cluster (2.514 Å) calculated at the same computational level. In fact, its molecular graph (Figure 1a) shows the presence of an Ag–Ag bond with the corresponding bond critical point. However, other electronic analysis carried out: ELF (Figure 1b) and NBO, do not indicate the presence of such bonds between the silver atoms due to the absence of the corresponding basin concomitantly with the Wiberg bond index of the Ag–Ag contact in $(PzAg)_2$—being 0.01, while that of Ag_2 is 0.92.

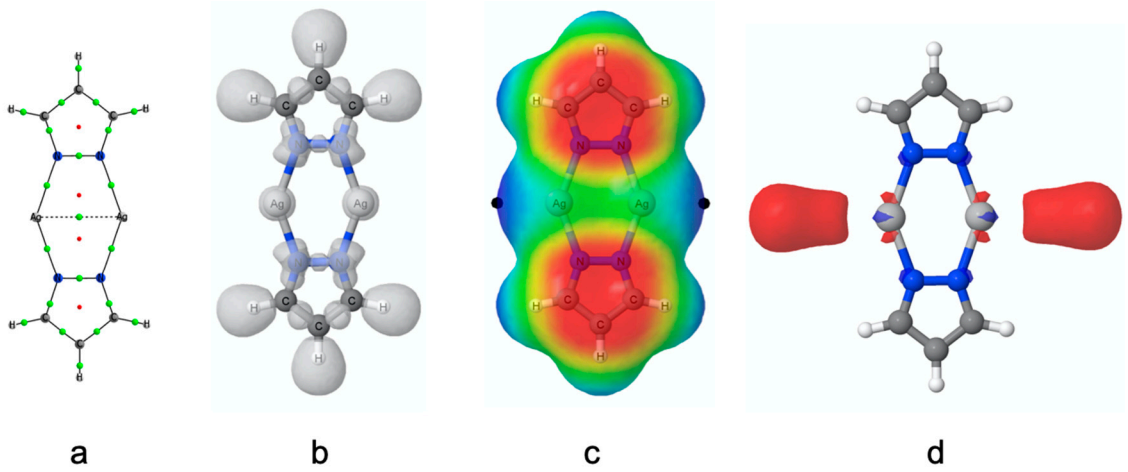

Figure 1. (**a**) Molecular graph, (**b**) electron localization function (ELF) at 0.7 isosurface value, (**c**) molecular electrostatic potential on the 0.001 au electron density isosurface (MESP) and (**d**) LUMO orbital of the $(PzAg)_2$ system. The green and red dots in the molecular graph indicate the location of the bond and ring critical points. The range of colors used in the MESP are red (MESP < –0.02 a.u.) and blue (MESP > 0.03 a.u.). The locations of the $V_{S,max}$ in the MESP are indicated with black dots.

The molecular electrostatic potential on the 0.001 au electron density isosurface (MESP) of the $(PzAg)_2$ system (Figure 1c) shows negative values above and below the pyrazole ring while the MESP in the extension of the CH and Ag–Ag bonds are positive. Moreover, the calculated maximum value on the MESP, $V_{S,max}$, in the vicinity of the silver atoms is +0.03 a.u. (marked with black dots) being the most positive value in the whole isosurface. Interestingly the LUMO orbital (Figure 1d) is solely associated to the Ag atoms and located in a region that coincides with the location of the $V_{S,max}$. Thus, the silver atoms of this molecule should act as a Lewis acid using both the electrostatic and orbital criteria.

3.3. The $(PzAg)_2$ Free Complex and the Effect of the Ag–Ag Distance on its Stability

The complex without ligands, $(PzAg)_2$, has in its minimum energy structure a distance between both silver atoms of 2.801 Å (Table S2) which is considerably shorter than any of the Ag–Ag distances found in the CSD. As we have already indicated in the CSD search, this distance is very sensitive to the environment (substituents of the pyrazole and ligands of the silver atoms) and can vary almost 1.0 Å from the shortest to the longest distance (3.392 and 4.305 Å, respectively). In order to explore the energetic penalty due to the elongation of the intramolecular Ag–Ag distance, the $(PzAg)_2$ system has been optimized while keeping fixed the Ag–Ag distance from 2.6 to 4.0 Å in steps of 0.2 Å (Table S2 and Figure 2). The energetic results indicate that lengthening the distance 1 Å, up to 3.8 Å, considerably decreases the stability of the system by 75 $kJ{\cdot}mol^{-1}$ which should be compensated by the interactions with the ligands.

3.4. Effect of the Ligands and Substituents on the Structure and Dissociation Energy (De)

After studying the free $(PzAg)_2$ system, the complexes with two ligands simultaneously interacting with the $(PzAg)_2$ system have been optimized, i.e., each silver atom interacts with a single ligand. The minimum structures obtained show that the interacting atom of the ligand is coplanar with the plane defined by the $(PzAg)_2$ system. The molecular graphs of two illustrative examples are shown in Figure 3 and the Cartesian coordinates of all of them were summarized in Table S3.

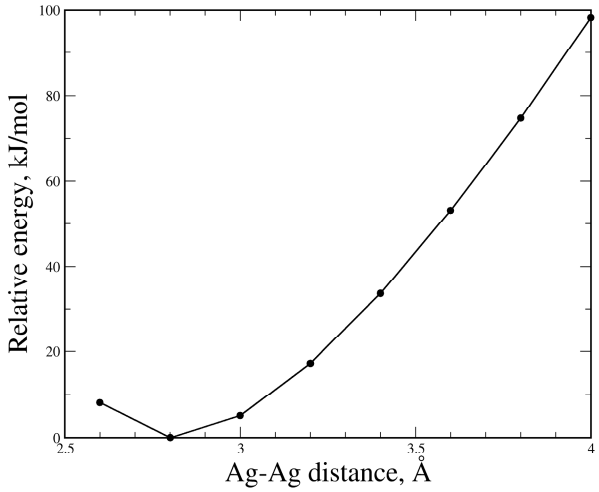

Figure 2. Relative energy vs. Ag–Ag distance in the $(PzAg)_2$ system.

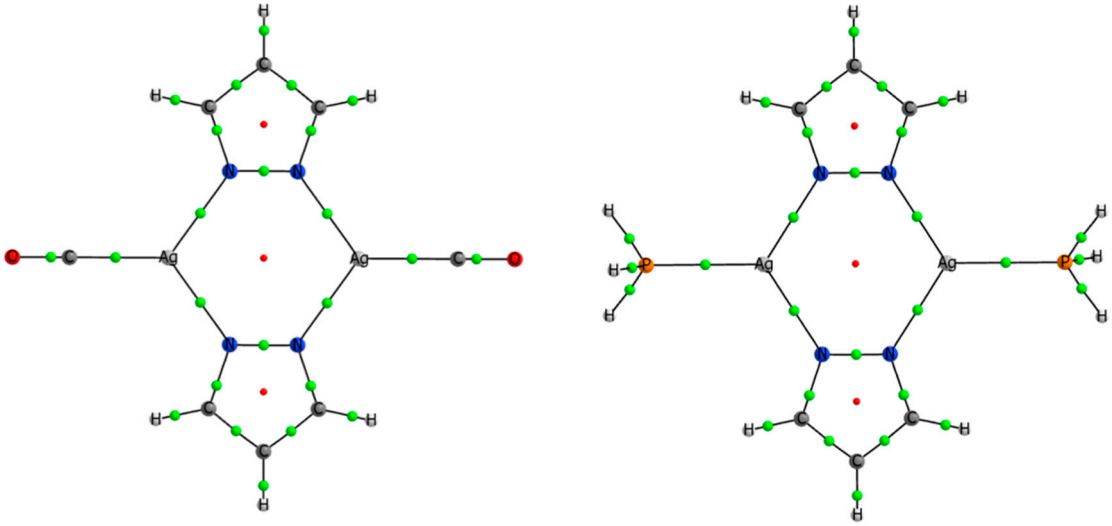

Figure 3. Molecular graph of the $(PzAg)_2(CO)_2$ and $(PzAg)_2(PH_3)_2$ complexes. The green and red dots indicate the location of the bond and ring critical points, respectively.

The complexation with ligands produces an elongation of the Ag–Ag distance up to 1.1 Å (Table 2) in agreement with the large variety of structures and the range of Ag–Ag distances found in the CSD search. For example, the crystal structure RATPAT (L = $(PPh_3)_2$) shows an Ag–Ag distance of 3.870 Å while in the calculated $(PzAg)_2(PH_3)_2$ complex this value is 3.689 Å. It is known that ligands coordinated by O, C or P atoms are strong, while those ligands coordinated by N atoms are weak. In the cases of CNH and HCN ligands are both -donors and -acceptors but the former is coordinated by the C atom while the latter is coordinated by the N atom. This results in larger dissociation energies for the $(PzAg)_2(CNH)_2$ complex in comparison with $(PzAg)_2(NCH)_2$. Similarly, this happens with CO and NH_3 ligands (both -donors), but while CO is a good -acceptor NH_3 is not, resulting in smaller values of De. In the case of the PH_3 ligand, it is both a -donor and -acceptor ligand, which is in agreement with the $(PzAg)_2(PH_3)_2$ complex, showing the second largest De. Chalcogen ligands, OH_2 (-donor) and SH_2 (-donor) present similar trends. In addition, it is also observed that the distance between both pyrazole rings decreases with the elongation of the Ag–Ag distance.

Table 2. Geometries and dissociation energy of $(PzAg)_2$ and $(PzAg)_2L_2$ systems.

Compound	Ag–Ag dist. (Å)	Pz-Pz dist. (Å) [a]	Ag-Z dist. (Å) [b]	De (kJ·mol^{-1})
$(PzAg)_2$	2.801	3.968	—	0.0
$(PzAg)_2(N_2)_2$	2.851	3.968	2.837	22.7
$(PzAg)_2(OH_2)_2$	2.908	3.994	2.630	54.5
$(PzAg)_2(NCH)_2$	3.078	3.933	2.425	56.3
$(PzAg)_2(SH_2)_2$	3.196	3.889	2.631	71.2
$(PzAg)_2(NH_3)_2$	3.255	3.905	2.358	91.7
$(PzAg)_2(PH_3)_2$	3.689	3.657	2.373	122.9
$(PzAg)_2(CO)_2$	3.845	3.519	1.998	90.0
$(PzAg)_2(CNH)_2$	3.880	3.534	2.018	136.6

[a] Measured as the distance between the smallest N–N distance in two pyrazole rings. [b] Z is the atom of L directly interacting with the silver atoms.

But, does this have any impact on the dissociation energy? Or, in other words, is there any relationship between the Ag–Ag intramolecular distance and the dissociation energy? The dissociation energy values corresponding to the $(PzAg)_2L_2$ complexes range between 23 kJ mol^{-1} for L = N_2 to 137 kJ mol^{-1} for L = CNH (Table 2). In general, despite observing a trend between the dissociation energy and the elongation of the Ag–Ag distance (Figure S1), no good fitting has been found (logarithmic fitting, R^2 = 0.73). The only outlier corresponds to the $(PzAg)_2(CO)_2$ complex, and when this point is neglected the fitting is more evident (R^2 = 0.90). A better exponential relationship has been found for the distance between the pyrazole rings vs. De (De = $5.55 \cdot e^{-0.114 Pz\text{-}Pz}$, R^2 = 0.92) which may suggest that the repulsion between pyrazole groups is partially responsible for the increase of the De energy but somehow compensated by the Ag–Ligand interaction.

The effect of the substituents (pyrazole ring) within the Ag–Ag distance and dissociation energies have been explored by considering four different pyrazole derivatives, R = H, 3,5-di(CH_3), 4-Cl and 4-NO_2. These isolated $(R\text{-}pzAg)_2$ systems have been fully optimized as well as in the presence of two phosphine molecules ligands with the results gathered in Table 3.

Table 3. Effect of the 3,5-dimethyl, 4-chloro and 4-nitro substituents (pyrazole ring) within the Ag–Ag distance and on the dissociation energy, De.

Compound	Ag–Ag dist. (Å)	De (kJ·mol^{-1})
$(DMepzAg)_2$	2.793	—-
$(PzAg)_2$	2.801	—-
$(4ClpzAg)_2$	2.819	—-
$(4NO_2pzAg)_2$	2.841	—-
$(DMepzAg)_2(PH_3)_2$	3.656	120.0
$(PzAg)_2(PH_3)_2$	3.689	122.9
$(4ClpzAg)_2(PH_3)_2$	3.730	135.1
$(4NO_2pzAg)_2(PH_3)_2$	3.782	150.8

In relation to the Ag–Ag distance in the isolated $(R\text{-}pzAg)_2$ systems, it increases in the following order: 3,5-di(CH_3) < H < 4-Cl < 4-NO_2 with a variation of 0.05 Å between both extremes. The same order was found within the $(R\text{-}pzAg)_2(PH_3)_2$ complexes but with a slightly larger range of 0.12 Å. This evolution was also found in the CSD search for complexes with three PPh_3 ligands: RATFEX (R = H) (3.706 Å) < ZIGRUF (R = 4-Cl) (3.707 Å) < ZIGSIU (R = 4-NO_2) (3.827 Å), and for complexes with four PPh_3 ligands: KIRVIX (R = H) (3.900 Å) < ZIGROG (R = 4-Cl) (4.209 Å) < ZIGSEQ (R = 4-NO_2) (4.305 Å).

The dissociation energies for the $(R\text{-}pzAg)_2(PH_3)_2$ complexes increase following the same trend of Ag–Ag distances (Table 3 and Figure S2). Furthermore, linear correlation with R^2 value of 0.97 was obtained between Ag–Ag distances and the De.

So far, only the systems with no ligands, $(R\text{-}pzAg)_2$, and complexes with two identical ligands, $(R\text{-}pzAg)_2L_2$, have been studied. In Table 4, the results corresponding to the complexes with 0, 1, 2 and 4 phosphine ligands bonded to $(PzAg)_2$ and $(4NO_2pzAg)_2$ systems are shown. In both series, the intramolecular Ag–Ag distance increases with the number of phosphine ligands bonded. When one PH_3 is bonded the increase in the Ag–Ag distance with respect to the isolated system is 0.286 and 0.311 Å for $(PzAg)_2$ and $(4NO_2pzAg)_2$ systems respectively. However, the change is two times larger when moving from 1 to 2 simultaneous ligands. Finally, the change is again moderate when 4 PH_3 ligands interacting with each Ag are considered. The CDS search also shows an increase of the Ag–Ag distance with the number of ligands. For example in the unsubstituted complexes (R=H) the Ag–Ag distance in RATFET (L = 3) is 3.706 Å and increases to 3.900 Å with four ligands (KIRXIV). This is also observed for substituted complexes with R=4-Cl: ZIGRUF (L = 3) 3.707 Å to ZIGROZ (L = 4) 4.209 Å and for R = $4NO_2$: ZIGSIU (L = 3) 3.827 Å) to ZIGSEQ (L = 4) 4.305 Å. In addition, it is interesting to notice that in complexes with four phosphines, the $(R\text{-}PzAg)_2$ system adopts a chair conformation (Figure 4) vs. the planar one observed with one or two ligands. The experimental Ag–Ag distances are longer than the calculated ones; this could be due to the fact that the ligand found in the crystals are bulkier (for instance PPh_3 vs. PH_3). This can be also related with the ratio of σ-donor/π-acceptor capacity in phosphorus ligands. In principle $P(CH_3)_3$ is a better σ-donor than PH_3, while the latter is a better π-acceptor [81]. However, the σ-donor/π-acceptor ratio indicates that the $P(CH_3)_3$ is a stronger ligand than PH_3. The same can be expected for PPh_3 and therefore the Ag–Ag distance will be larger for complexes that are PPh_3-coordinated compared with those for PH_3 ones.

Table 4. Effect of the number of ligands.

Compound	Number of Ls	Ag–Ag dist. (Å)	De (kJ·mol^{-1})	τ_4 index
$(PzAg)_2$	0	2.801	0.0	—
$(PzAg)_2(PH_3)$	1	3.087	64.2	—
$(PzAg)_2(PH_3)_2$	2	3.689	122.9	—
$(PzAg)_2(PH_3)_4$	4	3.798	214.5	0.81 & 0.83
$(4NO_2pzAg)_2$	0	2.841	0.0	—
$(4NO_2pzAg)_2(PH_3)$	1	3.152	77.4	
$(4NO_2pzAg)_2(PH_3)_2$	2	3.782	150.8	—
$(4NO_2pzAg)_2(PH_3)_4$	4	3.870	251.7	0.80 & 0.81

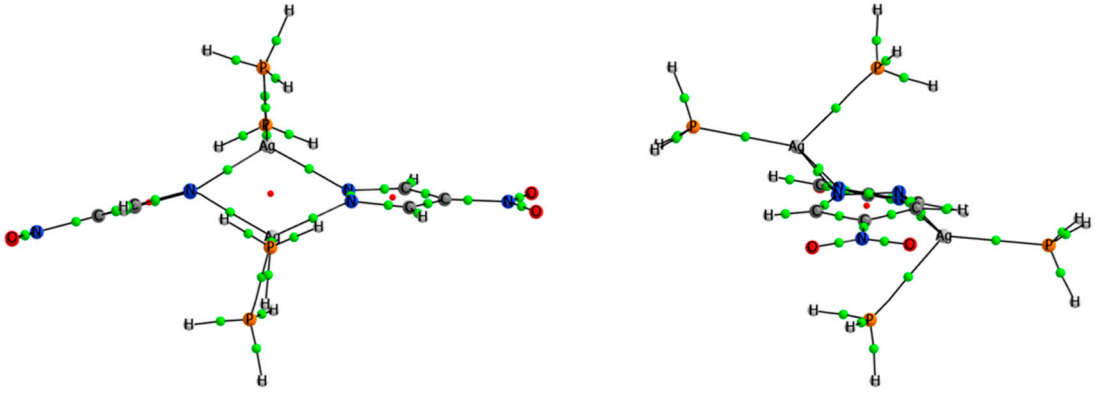

Figure 4. Two orthogonal views of the molecular graph of the $(4NO_2pzAg)_2(PH_3)_4$ complex.

Regarding the τ_4 index for $(PzAg)_2(PH_3)_4$ and $(4NO_2pzAg)_2(PH_3)_4$: the values for both Ag are 0.81 and 0.83 respectively, in between of those found for ZIGSAM (0.78) and ZIGROZ (0.89) crystal structures.

The values of De show an anticooperativity effect as the number of phosphines increases, thus the De's of the systems with two phosphines are smaller than twice the corresponding ones with one phosphine and the same happens when the results between the systems with two and four

phosphines are compared. Looking at the values shown in Table 4, $(PzAg)_2(PH_3)$ complex yields a De of 64.2 kJ·mol^{-1}, whereas $(PzAg)_2(PH_3)_2$ complex's is 122.9 kJ·mol^{-1}, 5.5 kJ·mol^{-1} smaller than twice the corresponding value for $(PzAg)_2(PH_3)$. This is an indication of an anti-cooperativity effect, which is more evident when $(PzAg)_2(PH_3)_4$ complex is taken into account (~42 kJ·mol^{-1} less than four times the De of $(PzAg)_2(PH_3)$). This is also observed for $(4NO_2pzAg)_2$ and the corresponding complexes, but the differences, i.e., the anti-cooperativity, is rather smaller (4.0 kJ·mol^{-1}) for $(4NO_2pzAg)_2(PH_3)_2$ and slightly larger for $(4NO_2pzAg)_2(PH_3)_4$ (57.9 kJ·mol^{-1}).

3.5. Electron Density

The critical points of the electron density of all systems have been characterized using the quantum theory of atoms in molecules (QTAIM) method. As aforementioned, a bond critical point (BCP) is obtained for the $(PzAg)_2$ system in between both Ag atoms. A similar feature has been obtained for all the systems with Ag–Ag distances shorter than 3.3 Å. The electron density values, ρ_{BCP}, of this BCP (Table S4) range between 0.032 and 0.014 a.u., with positive values of the Laplacian, $\nabla^2\rho$ (between 0.098 and 0.041 a.u.) and negative values of the total energy density, H_{BCP}, except for the system with the largest Ag–Ag bond in this set ($(PzAg)_2(NH_3)_2$). Excellent exponential relationships are obtained between the ρ_{BCP} and $\nabla^2\rho_{BCP}$ and the interatomic distance in agreement with previous reports (Figure 5) [82,83].

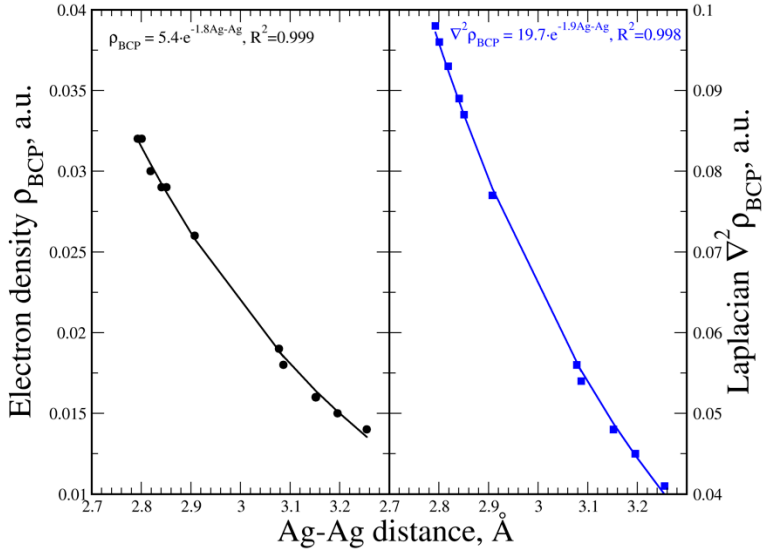

Figure 5. Electron density, ρ_{BCP}, and Laplacian, $\nabla^2\rho_{BCP}$, vs. the Ag–Ag distance (Å). The fitted exponential relationships are shown.

Concering the Ag–L bonds, the corresponding bond critical points between the silver atom and the different ligands have been gathered in Table S5. In all the cases, the interactions exhibit positive values of the $\nabla^2\rho_{BCP}$ and negative values of H_{BCP}, which indicates a partial covalent character of the bond formed [84,85]. The only exception corresponds to the weakest complex, $(PzAg)_2(N_2)_2$, which shows a small positive H_{BCP} value. The 14 unique Ag–P contacts found in this set show similar relationships between ρ_{BCP} and $\nabla^2\rho_{BCP}$ vs. the Ag–P distance to those previously mentioned for Ag–Ag BCPs.

3.6. Magnetic Properties and Aromaticity

Among the different nuclei suitable for NMR spectra present in these systems (^{1}H, ^{13}C and ^{15}N), ^{109}Ag is the one with the largest range of chemical shifts. The calculated ^{109}Ag chemical shielding for all the systems studied in this article are listed in Table 5. It is worth noting that upon complexation ^{109}Ag can change its chemical shielding by more than 1200 ppm to lower field, from 3765 ppm ($(PzAg)_2$) to 2550.48 ppm ($(PzAg)_2(PH_3)_4$). Furthermore, a good relationship between the chemical shielding

and the intramolecular Ag–Ag distance (only for complexes with two ligands) was found (Figure S3). Unfortunatelly, there are no experimental data on $(PzAg)_2$ compounds but a recent report on $(PzAg)_3$ derivatives show that the methodology used here provides δ^{109}Ag values within 10 ppm of the experimental ones [46].

Table 5. ^{109}Ag absolute chemical shielding (σ, ppm) and nuclear-independent chemical shift (NICS) values (ppm) of the six-membered and pyrazole rings.

System	σ^{109}Ag (ppm)	6-Membered Ring		Pz Ring	
		NICS(0)	NICS(1)	NICS(0)	NICS(1)
$(PzAg)_2$	3765.7	−7.39	−1.84	−13.06	−10.97
$(PzAg)_2(N_2)_2$	3648.3	−7.17	−1.70	−12.70	−10.95
$(PzAg)_2(OH_2)_2$	3752.8	−5.82	−1.48	−12.88	−11.22
$(PzAg)_2(NCH)_2$	3515.5	−4.76	−1.10	−12.67	−11.03
$(PzAg)_2(SH_2)_2$	3288.3	−3.55	−0.65	−12.75	−11.04
$(PzAg)_2(NH_3)_2$	3511.9	−2.40	−0.38	−12.74	−11.12
$(PzAg)_2(PH_3)_2$	2900.9	−0.14	0.12	−12.27	−11.11
$(PzAg)_2(CO)_2$	2706.9	−0.56	−0.33	−12.37	−11.13
$(PzAg)_2(CNH)_2$	2825.4	−0.16	−0.12	−12.29	−11.16
$(DMepzAg)_2$	3720.4	−7.98	−2.23	−10.50	−9.34
$(4ClpzAg)_2$	3815.9	−7.11	−1.75	−12.62	−9.98
$(4NO_2pzAg)_2$	3835.5	−6.95	−1.72	−11.98	−9.50
$(DMepzAg)_2(PH_3)_2$	2893.1	−0.73	−0.25	−9.32	−9.29
$(4ClpzAg)_2(PH_3)_2$	2954.4	−0.17	0.07	−11.74	−10.09
$(4NO_2pzAg)_2(PH_3)_2$	3010.2	0.12	0.19	−10.81	−9.41
$(PzAg)_2(PH_3)_4$	2561.6				
	2550.5				
$(4NO_2pzAg)_2(PH_3)_4$	2619.5				
	2627.7				

In order to explore the potential aromaticity of the six membered ring formed by the nitrogen atoms of the pyrazoles and the two silver atoms, the NICS(0) and NICS(1) have been calculated (Table 5). Despite NICS isotropic values being widely used and well established, there is still a controversy about the reliability of NICS values for assessment of the aromaticity of certain molecules [86,87]. Nevertheless, and following our previous experience, the isotropic values have in several cases been shown to present an accurate description of the aromatic behaviour in poly-aromatic systems [88–90].

Despite almost all the systems studied presenting negative NICS(0) values in the six-membered ring, only those with short Ag–Ag distances (2.8–3.0 Å) present very negative values close to the benzene molecule (−8 ppm) [91], and, also, those NICS(0) values decrease in absolute value as the Ag–Ag distance increases. NICS(1) are smaller, in absolute value, than NICS(0), but follow the same trend as the latter. Also, NICS(1) are very small compared with benzene ones (−10.2 ppm) [91] which suggest non-aromatic character. But, those values should be taken carefully, since the two silver atoms are very close and the proximity of the nuclei may affect the NICS(0) measure. To provide a further insight on this, Figure 6 clearly shows that there is a unique dependence between the NICS(0) and NICS(1), the distance between the location where the NICS is measured and the silver atom. The scan of the NICS values for $(PzAg)_2$ from 0 to 2.0 Å above the centre of the six-membered ring (Table S6) have also been plotted in Figure 6 showing a similar evolution to the NICS(0) and NICS(1) of the rest of the molecules. This indicates that, as aforementioned, this ring is not aromatic but the NICS values obtained are somehow affected by the proximity of the silver atom.

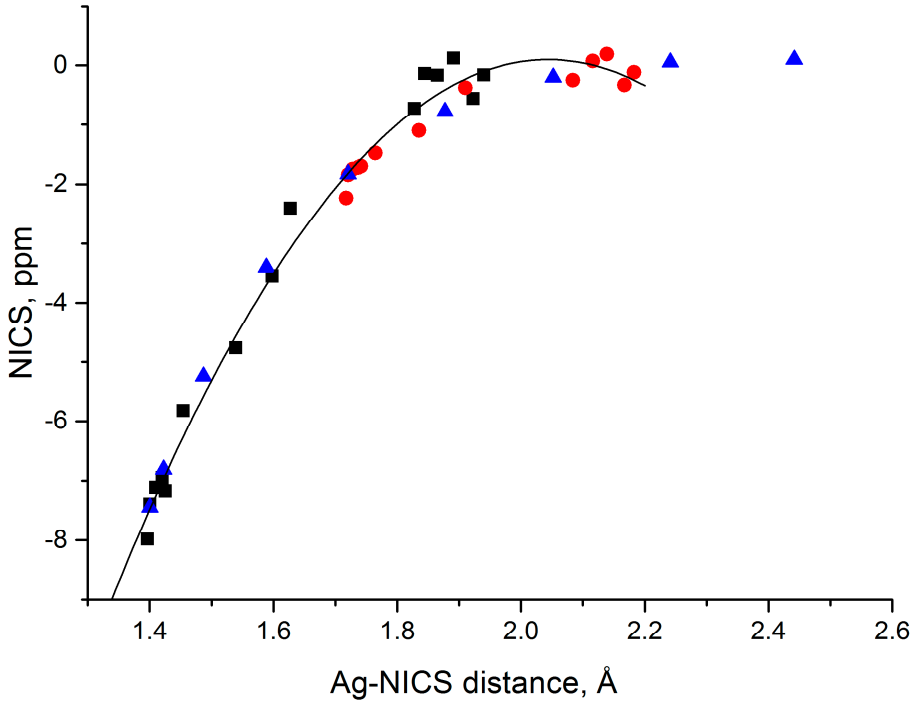

Figure 6. NICS(0), black squares, and NICS(1) values, red dots, of the six-membered ring versus the distance between the silver atom and the location where the NICS were measured (Ag–NICS distance). The blue triangles representes the NICS values for the $(PzAg)_2$ scan between 0.0 and 2.0 Å. The second order polynomial equation fitting the values of the NICS(0) and NICS(1) has an R^2 value of 0.989.

In contrast the NICS(0) and NICS(1) values of the pyrazole rings are negative and large in all cases and very close to the ones obtained by Kusakiewicz-Dawid (−13.5 and −11.4 ppm respectively) [92].

On the other hand, the substituents on the pyrazole ring have a greater effect on the NICS values than the different ligands on the $(PzAg)_2L_2$ complexes, most likely due to changes in the electron density on the ring current electrons. For instance the NICS(0) in the $(Rpz\text{-}Ag)_2$ systems ranges between −10.5 and −13.1 ppm while in the $(PzAg)_2L_2$ complexes it is between −12.3 and −13.1 ppm.

4. Conclusions

A theoretical study and CSD search of the different effects provoked by substituents and ligands upon complexation with dinuclear Ag(I) pyrazolates has been carried out and the structural, energetic, electron density and magnetic features analyzed.

The CSD search shows a great variability of the Ag–Ag distance in the crystal structures. These results have been rationalized based on the number of ligand interactions with the Ag atoms and the substituents of the pyrazole ring.

In the isolated $(PzAg)_2$ system, it was observed that for Ag–Ag the longer the distance, the lesser the stability of the unsubstituted complex with no ligands. This decrease in the stability is somehow compensated by the ligands upon complexation.

Furthermore, complexation with ligands through the Ag atoms increases the intramolecular distance Ag–Ag. In fact, considering the PH_3 ligand, the increase of the Ag–Ag distance was found moderate when going from no ligand to one ligand. However, when two simultaneous PH_3 are interacting, the Ag–Ag distance increases dramatically. Nevertheless, when four PH_3 are considered, the increase is again moderate.

In terms of the QTAIM analysis, it is noteworthy the presence of a BCP between both Ag atoms among all the systems with Ag–Ag distances shorter than 3.3 Å.

Finally, regarding the aromatic/non-aromatic properties, six-membered rings containing the Ag–Ag motif show negative NICS values but those reveal a non-aromatic character mainly affected by

the proximity of the Ag nuclei. This was confirmed by the relationship found between the NICS values and the Ag–NICS distance. On the other hand, pyrazole rings maintain their aromatic behaviour with slight changes.

Supplementary Materials: The following are available online at http://www.mdpi.com/2073-4352/10/2/137/s1, Table S1: Two simplified views of the structures found in the CSD search, Table S2. Effect of the Ag(I)–Ag(I) distance (Å) on the relative energy (kJ·mol^{-1}) of the $(PzAg)_2$ system, Table S3: Cartesian coordinates (Å) of the optimized systems at MP2/jul-cc-pVDZ/jul-cc-pVDZ-PP level, Figure S1: Relative energy vs. Ag–Ag distance in the $(PzAg)_2$ system, Figure. S2: De (kJ·mol^{-1}) vs. Ag–Ag dist. (Å) in the $(PzAg)_2L_2$ complexes, Figure S3: De (kJ·mol^{-1}) vs. Ag–Ag dist. (Å) in the $(R\text{-}pzAg)_2(PH_3)_2$ complexes, Table S4: Distance (Å) and electron density properties (au) of the Ag–Ag BCPs, Table S5: Distance (Å) and electron density properties (au) of the Ag–L BCPs, Figure S4: ^{109}Ag chemical shielding vs. Ag–Ag distance in the $(PzAg)_2L_2$ complexes. Table S6. NICS values (ppm) from 0.0 to 2.0 Å of the center of the 6-membered ring in $(PzAg)_2$.

Author Contributions: Conceptualization and project design, I.A., J.E.; resources, I.A., C.T., G.S.-S, data curation, I.A, J.E, C.T., G.S.-S., writing—original draft preparation, I.A, J.E, C.T., G.S.-S.; writing—review and editing, I.A, J.E, C.T., G.S.-S.; funding acquisition, I.A. C.T.; All authors have read and agreed to the published version of the manuscript.

Funding: This work was carried out with financial support from the Spanish Ministerio de Ciencia, Innovación y Universidades (Projects PGC2018-094644-B-C2) and Dirección General de Investigación e Innovación de la Comunidad de Madrid (PS2018/EMT-4329 AIRTEC-CM), and Science Foundation of Ireland (SFI), grant number 18/SIRG/5517.

Acknowledgments: We are grateful to the Irish Centre for High-End Computing (ICHEC) and CTI(CSIC) for the provision of computational facilities. We are also grateful to Dr Lee O'Riordan for his continuous support and help.

Conflicts of Interest: The authors declare no conflict of interest.

References

1. Cavallo, G.; Metrangolo, P.; Pilati, T.; Resnati, G.; Terraneo, G. Naming Interactions from the Electrophilic Site. *Cryst. Growth Des.* **2014**, *14*, 2697–2702. [CrossRef]
2. Politzer, P.; Murray, J.S. *An Overview of σ-Hole Bonding, an Important and Widely-Occurring Noncovalent Interaction Practical Aspects of Computational Chemistry*; Leszczynski, J., Shukla, M.K., Eds.; Springer: Dordrecht, The Netherlands, 2010; pp. 149–163.
3. Politzer, P.; Murray, J.S.; Clark, T. Halogen bonding: An electrostatically-driven highly directional noncovalent interaction. *PCCP* **2010**, *12*, 7748–7757. [CrossRef] [PubMed]
4. Politzer, P.; Murray, J.S.; Clark, T. Halogen bonding and other [sigma]-hole interactions: A perspective. *PCCP* **2013**, *15*, 11178–11189. [CrossRef] [PubMed]
5. Bauzá, A.; Mooibroek, T.J.; Frontera, A. The Bright Future of Unconventional σ/π-Hole Interactions. *ChemPhysChem* **2015**, *16*, 2496–2517. [CrossRef] [PubMed]
6. Murray, J.; Lane, P.; Clark, T.; Riley, K.; Politzer, P. σ-Holes, π-holes and electrostatically-driven interactions. *J. Mol. Model.* **2012**, *18*, 541–548. [CrossRef] [PubMed]
7. Solimannejad, M.; Ramezani, V.; Trujillo, C.; Alkorta, I.; Sánchez-Sanz, G.; Elguero, J. Competition and Interplay between σ-Hole and π-Hole Interactions: A Computational Study of 1:1 and 1:2 Complexes of Nitryl Halides (O2NX) with Ammonia. *J. Phys. Chem. A* **2012**, *116*, 5199–5206. [CrossRef]
8. Grabowski, S.J. Hydrogen bonds, and σ-hole and π-hole bonds—Mechanisms protecting doublet and octet electron structures. *PCCP* **2017**, *19*, 29742–29759. [CrossRef]
9. Bauzá, A.; Mooibroek, T.J.; Frontera, A. Directionality of π-holes in nitro compounds. *Chem. Commun.* **2015**, *51*, 1491–1493. [CrossRef]
10. Zierkiewicz, W.; Michalczyk, M.; Wysokiński, R.; Scheiner, S. On the ability of pnicogen atoms to engage in both σ and π-hole complexes. Heterodimers of ZF2C6H5 (Z = P, As, Sb, Bi) and NH3. *J. Mol. Model.* **2019**, *25*, 152. [CrossRef]
11. Azofra, L.; Alkorta, I.; Scheiner, S. Noncovalent interactions in dimers and trimers of SO3 and CO. *Theor. Chem. Acc.* **2014**, *133*, 1–8. [CrossRef]

12. Blanco, F.; Alkorta, I.; Rozas, I.; Solimannejad, M.; Elguero, J. A theoretical study of the interactions of NF3 with neutral ambidentate electron donor and acceptor molecules. *PCCP* **2011**, *13*, 674–683. [CrossRef] [PubMed]
13. Alkorta, I.; Elguero, J.; Del Bene, J.E. Exploring the PX3:NCH and PX3:NH3 potential surfaces, with X=F, Cl, and Br. *Chem. Phys. Lett.* **2015**, *641*, 84–89. [CrossRef]
14. Bauzá, A.; Mooibroek, T.J.; Frontera, A. σ-Hole Opposite to a Lone Pair: Unconventional Pnicogen Bonding Interactions between ZF3 (Z=N, P, As, and Sb) Compounds and Several Donors. *ChemPhysChem* **2016**, *17*, 1608–1614. [CrossRef] [PubMed]
15. Stenlid, J.H.; Brinck, T. Extending the σ-Hole Concept to Metals: An Electrostatic Interpretation of the Effects of Nanostructure in Gold and Platinum Catalysis. *JACS* **2017**, *139*, 11012–11015. [CrossRef]
16. Shahi, A.; Arunan, E. Hydrogen bonding, halogen bonding and lithium bonding: An atoms in molecules and natural bond orbital perspective towards conservation of total bond order, inter- and intra-molecular bonding. *PCCP* **2014**, *16*, 22935–22952. [CrossRef]
17. Solimannejad, M.; Rabbani, M.; Ahmadi, A.; Esrafili, M.D. Cooperative and diminutive interplay between the sodium bonding with hydrogen and dihydrogen bondings in ternary complexes of NaC3N with HMgH and HCN (HNC). *Mol. Phys.* **2014**, *112*, 2017–2022. [CrossRef]
18. Yáñez, M.; Sanz, P.; Mó, O.; Alkorta, I.; Elguero, J. Beryllium Bonds, Do They Exist? *J. Chem. Theor. Comput.* **2009**, *5*, 2763–2771. [CrossRef]
19. Alkorta, I.; Legon, A.C. Non-Covalent Interactions Involving Alkaline-Earth Atoms and Lewis Bases B: An ab Initio Investigation of Beryllium and Magnesium Bonds, B·MR2 (M = Be or Mg, and R = H, F or CH3). *Inorganics* **2019**, *7*, 35. [CrossRef]
20. Montero-Campillo, M.M.; Mó, O.; Yáñez, M.; Alkorta, I.; Elguero, J. Chapter Three—The beryllium bond. In *Advances in Inorganic Chemistry*; van Eldik, R., Puchta, R., Eds.; Academic Press: Cambridge, MA, USA, 2019; Volume 73, pp. 73–121.
21. Frontera, A.; Bauzá, A. Regium–π bonds: An Unexplored Link between Noble Metal Nanoparticles and Aromatic Surfaces. *Chem. Eur. J.* **2018**, *24*, 7228–7234. [CrossRef]
22. Zierkiewicz, W.; Michalczyk, M.; Scheiner, S. Regium bonds between Mn clusters (M = Cu, Ag, Au and n = 2–6) and nucleophiles NH3 and HCN. *PCCP* **2018**, *20*, 22498–22509. [CrossRef]
23. Legon, A.C.; Walker, N.R. What's in a name? 'Coinage-metal' non-covalent bonds and their definition. *PCCP* **2018**, *20*, 19332–19338. [CrossRef] [PubMed]
24. Grabowski, S.J. Triel Bonds, π-Hole-π-Electrons Interactions in Complexes of Boron and Aluminium Trihalides and Trihydrides with Acetylene and Ethylene. *Molecules* **2015**, *20*, 11297–11316. [CrossRef] [PubMed]
25. Alkorta, I.; Rozas, I.; Elguero, J. Molecular Complexes between Silicon Derivatives and Electron-Rich Groups. *J. Phys. Chem. A* **2001**, *105*, 743–749. [CrossRef]
26. Alkorta, I.; Blanco, F.; Elguero, J.; Dobado, J.A.; Ferrer, S.M.; Vidal, I. Carbon·Carbon Weak Interactions. *J. Phys. Chem. A* **2009**, *113*, 8387–8393. [CrossRef] [PubMed]
27. Bauzá, A.; Mooibroek, T.J.; Frontera, A. Tetrel-Bonding Interaction: Rediscovered Supramolecular Force? *Angew. Chem. Int. Ed.* **2013**, *52*, 12317–12321. [CrossRef] [PubMed]
28. Grabowski, S.J. Tetrel bond-[sigma]-hole bond as a preliminary stage of the SN2 reaction. *Phys. Chem. Chem. Phys.* **2014**, *16*, 1824–1834. [CrossRef]
29. Del Bene, J.E.; Alkorta, I.; Elguero, J. The Pnicogen Bond in Review: Structures, Binding Energies, Bonding Properties, and Spin-Spin Coupling Constants of Complexes Stabilized by Pnicogen Bonds. In *Noncovalent Forces*; Scheiner, S., Ed.; Springer International Publishing: Cham, Switzerland, 2015; pp. 191–263. [CrossRef]
30. Zahn, S.; Frank, R.; Hey-Hawkins, E.; Kirchner, B. Pnicogen Bonds: A New Molecular Linker? *Chem. Eur. J.* **2011**, *17*, 6034–6038. [CrossRef]
31. Scheiner, S. The Pnicogen Bond: Its Relation to Hydrogen, Halogen, and Other Noncovalent Bonds. *Acc. Chem. Res.* **2013**, *46*, 280–288. [CrossRef]
32. Minyaev, R.M.; Minkin, V.I. Theoretical study of O- > X (S, Se, Te) coordination in organic compounds. *Can. J. Chem.* **1998**, *76*, 776–788. [CrossRef]
33. Wang, W.; Ji, B.; Zhang, Y. Chalcogen Bond: A Sister Noncovalent Bond to Halogen Bond. *J. Phys. Chem. A* **2009**, *113*, 8132–8135. [CrossRef]
34. Sanz, P.; Yáñez, M.; Mó, O. Competition between X···H···Y Intramolecular Hydrogen Bonds and X····Y (X = O, S, and Y = Se, Te) Chalcogen−Chalcogen Interactions. *J. Phys. Chem. A* **2002**, *106*, 4661–4668. [CrossRef]

35. Azofra, L.M.; Alkorta, I.; Scheiner, S. Strongly bound noncovalent (SO3)n:H2CO complexes (n = 1, 2). *Phys. Chem. Chem. Phys.* **2014**, *16*, 18974–18981. [CrossRef] [PubMed]
36. Legon, A.C. Prereactive Complexes of Dihalogens XY with Lewis Bases B in the Gas Phase: A Systematic Case for the Halogen Analogue B···XY of the Hydrogen Bond B···HX. *Angew. Chem. Int. Ed.* **1999**, *38*, 2686–2714. [CrossRef]
37. Cavallo, G.; Metrangolo, P.; Milani, R.; Pilati, T.; Priimagi, A.; Resnati, G.; Terraneo, G. The Halogen Bond. *Chem. Rev.* **2016**, *116*, 2478–2601. [CrossRef] [PubMed]
38. Bauzá, A.; Frontera, A. Aerogen Bonding Interaction: A New Supramolecular Force? *Angew. Chem. Int. Ed.* **2015**, *54*, 7340–7343. [CrossRef] [PubMed]
39. Halldin Stenlid, J.; Johansson, A.J.; Brinck, T. σ-Holes and σ-lumps direct the Lewis basic and acidic interactions of noble metal nanoparticles: Introducing regium bonds. *PCCP* **2018**, *20*, 2676–2692. [CrossRef]
40. Li, Q.; Li, H.; Li, R.; Jing, B.; Liu, Z.; Li, W.; Luan, F.; Cheng, J.; Gong, B.; Sun, J. Influence of Hybridization and Cooperativity on the Properties of Au-Bonding Interaction: Comparison with Hydrogen Bonds. *J. Phys. Chem. A* **2011**, *115*, 2853–2858. [CrossRef]
41. Sánchez-Sanz, G.; Alkorta, I.; Elguero, J.; Yáñez, M.; Mó, O. Strong interactions between copper halides and unsaturated systems: New metallocycles? Or the importance of deformation. *PCCP* **2012**, *14*, 11468–11477. [CrossRef]
42. Zhang, J.; Wang, Z.; Liu, S.; Cheng, J.; Li, W.; Li, Q. Synergistic and diminutive effects between triel bond and regium bond: Attractive interactions between π-hole and σ-hole. *Appl. Organomet. Chem.* **2019**, *33*, e4806. [CrossRef]
43. Sánchez-Sanz, G.; Trujillo, C.; Alkorta, I.; Elguero, J. Understanding Regium Bonds and their Competition with Hydrogen Bonds in Au2:HX Complexes. *ChemPhysChem* **2019**, *20*, 1572–1580. [CrossRef]
44. Wang, R.; Yang, S.; Li, Q. Coinage-Metal Bond between [1.1.1]Propellane and M2/MCl/MCH3 (M = Cu, Ag, and Au): Cooperativity and Substituents. *Molecules* **2019**, *24*, 2601. [CrossRef] [PubMed]
45. Zheng, B.; Liu, Y.; Wang, Z.; Zhou, F.; Liu, Y.; Ding, X.; Lu, T. Regium bonds formed by MX (M = Cu, Ag, Au; X = F, Cl, Br) with phosphine-oxide/phosphinous acid: Comparisons between oxygen-shared and phosphine-shared complexes. *Mol. Phys.* **2019**, *117*, 2443–2455. [CrossRef]
46. Alkorta, I.; Elguero, J.; Dias, H.V.R.; Parasar, D.; Martín-Pastor, M. An experimental and computational NMR study of organometallic nine-membered rings: Trinuclear silver(I) complexes of pyrazolate ligands. *Magn. Reson. Chem.* **2020**. [CrossRef] [PubMed]
47. Allen, F. The Cambridge Structural Database: A quarter of a million crystal structures and rising. *Acta Crystallogr. Sect. B Struct. Sci.* **2002**, *58*, 380–388. [CrossRef]
48. Pople, J.A.; Binkley, J.S.; Seeger, R. Theoretical models incorporating electron correlation. *Int. J. Quantum Chem.* **1976**, *10*, 1–19. [CrossRef]
49. Krishnan, R.; Pople, J.A. Approximate fourth-order perturbation theory of the electron correlation energy. *Int. J. Quantum Chem.* **1978**, *14*, 91–100. [CrossRef]
50. Bartlett, R.J.; Silver, D.M. Many-body perturbation theory applied to electron pair correlation energies. I. Closed-shell first-row diatomic hydrides. *J. Chem. Phys.* **1975**, *62*, 3258–3268. [CrossRef]
51. Bartlett, R.J.; Purvis, G.D. Many-body perturbation theory, coupled-pair many-electron theory, and the importance of quadruple excitations for the correlation problem. *Int. J. Quantum Chem.* **1978**, *14*, 561–581. [CrossRef]
52. Del Bene, J.E. Proton affinities of ammonia, water, and hydrogen fluoride and their anions: A quest for the basis-set limit using the Dunning augmented correlation-consistent basis sets. *J. Phys. Chem.* **1993**, *97*, 107–110. [CrossRef]
53. Dunning, T.H. Gaussian-Basis Sets for Use in Correlated Molecular Calculations. I. The Atoms Boron through Neon and Hydrogen. *J. Chem. Phys.* **1989**, *90*, 1007–1023. [CrossRef]
54. Woon, D.E.; Dunning, T.H. Gaussian basis sets for use in correlated molecular calculations. V. Core-valence basis sets for boron through neon. *J. Chem. Phys.* **1995**, *103*, 4572–4585. [CrossRef]
55. Peterson, A.K.; Puzzarini, C. Systematically convergent basis sets for transition metals. II. Pseudopotential-based correlation consistent basis sets for the group 11 (Cu, Ag, Au) and 12 (Zn, Cd, Hg) elements. *Theor. Chem. Acc.* **2005**, *114*, 283–296. [CrossRef]

56. Frisch, M.J.T.; Schlegel, H.B.; Scuseria, G.E.; Robb, M.A.; Cheeseman, J.R.; Scalmani, G.; Barone, V.; Petersson, G.A.; Nakatsuji, H.; Li, X.; et al. *Gaussian 16, Revision A.03*; Gaussian Inc.: Wallingford, CT, USA, 2016.
57. Lu, T.; Chen, F. Multiwfn: A multifunctional wavefunction analyzer. *J. Comput. Chem.* **2012**, *33*, 580–592. [CrossRef] [PubMed]
58. Jmol: An Open-Source Java Viewer for Chemical Structures in 3D. Available online: http://www.jmol.org/ (accessed on 24 February 2020).
59. Bader, R.F.W. *Atoms in Molecules: A Quantum Theory*; Clarendon Press: Oxford, UK, 1990.
60. Bader, R.F.W. A quantum theory of molecular structure and its applications. *Chem. Rev.* **1991**, *91*, 893–928. [CrossRef]
61. Popelier, P.L.A. *Atoms in Molecules An Introduction*; Prentice Hall: Harlow, UK, 2000.
62. Matta, C.F.; Boyd, R.J. *The Quantum Theory of Atoms in Molecules: From Solid State to DNA and Drug Design*; Wiley-VCH: Weinheim, Germany, 2007.
63. Keith, T.A. *AIMAll, 17.11.14 B*; Version 17.11.14 B; TK Gristmill Software: Overland Park, KS, USA, 2017.
64. Reed, A.E.; Curtiss, L.A.; Weinhold, F. Intermolecular Interactions from a Natural Bond Orbital, Donor-Acceptor Viewpoint. *Chem. Rev.* **1988**, *88*, 899–926. [CrossRef]
65. Noury, S.; Krokidis, X.; Fuster, F.; Silvi, B. *TopMod Package*; Universite Pierre et Marie Curie: Paris, France, 1997.
66. Silvi, B.; Savin, A. Classification of chemical bonds based on topological analysis of electron localization functions. *Nature* **1994**, *371*, 683–686. [CrossRef]
67. Savin, A.; Silvi, B.; Coionna, F. Topological analysis of the electron localization function applied to delocalized bonds. *Can. J. Chem.* **1996**, *74*, 1088–1096. [CrossRef]
68. Schreckenbach, G.; Ziegler, T. Calculation of NMR Shielding Tensors Using Gauge-Including Atomic Orbitals and Modern Density Functional Theory. *J. Phys. Chem.* **1995**, *99*, 606–611. [CrossRef]
69. Lenthe, E.V.; Baerends, E.J.; Snijders, J.G. Relativistic regular two-component Hamiltonians. *J. Chem. Phys.* **1993**, *99*, 4597–4610. [CrossRef]
70. Vosko, S.H.; Wilk, L.; Nusair, M. Accurate spin-dependent electron liquid correlation energies for local spin density calculations: A critical analysis. *Can. J. Phys.* **1980**, *58*, 1200–1211. [CrossRef]
71. Becke, A.D. Density-functional exchange-energy approximation with correct asymptotic behavior. *Phys. Rev. A* **1988**, *38*, 3098–3100. [CrossRef] [PubMed]
72. Perdew, J.P. Density-functional approximation for the correlation energy of the inhomogeneous electron gas. *Phys. Rev. B* **1986**, *33*, 8822–8824. [CrossRef] [PubMed]
73. Van Lenthe, E.; Baerends, E.J. Optimized Slater-type basis sets for the elements 1–118. *J. Comput. Chem.* **2003**, *24*, 1142–1156. [CrossRef] [PubMed]
74. Schleyer, P.V.; Maerker, C.; Dransfeld, A.; Jiao, H.J.; Hommes, N.J.R.V. Nucleus-independent chemical shifts: A simple and efficient aromaticity probe. *JACS* **1996**, *118*, 6317–6318. [CrossRef]
75. Stanger, A. Nucleus-Independent Chemical Shifts (NICS): Distance Dependence and Revised Criteria for Aromaticity and Antiaromaticity. *J. Org. Chem.* **2006**, *71*, 883–893. [CrossRef]
76. Gershoni-Poranne, R.; Stanger, A. Magnetic criteria of aromaticity. *Chem. Soc. Rev.* **2015**, *44*, 6597–6615. [CrossRef]
77. Te Velde, G.; Bickelhaupt, F.M.; Baerends, E.J.; Fonseca Guerra, C.; van Gisbergen, S.J.A.; Snijders, J.G.; Ziegler, T. Chemistry with ADF. *J. Comput. Chem.* **2001**, *22*, 931–967. [CrossRef]
78. Omary, M.A.; Rawashdeh-Omary, M.A.; Diyabalanage, H.V.K.; Dias, H.V.R. Blue Phosphors of Dinuclear and Mononuclear Copper(I) and Silver(I) Complexes of 3,5-Bis(trifluoromethyl)pyrazolate and the Related Bis(pyrazolyl)borate. *Inorg. Chem.* **2003**, *42*, 8612–8614. [CrossRef]
79. Yang, L.; Powell, D.R.; Houser, R.P. Structural variation in copper(i) complexes with pyridylmethylamide ligands: Structural analysis with a new four-coordinate geometry index, τ4. *Dalton Trans.* **2007**, 955–964. [CrossRef]
80. Kandel, S.; Stenger-Smith, J.; Chakraborty, I.; Raptis, R.G. Syntheses and X-ray crystal structures of a family of dinuclear silver(I)pyrazolates: Assessment of their antibacterial efficacy against P. aeruginosa with a soft tissue and skin infection model. *Polyhedron* **2018**, *154*, 390–397. [CrossRef]
81. Mitoraj, M.P.; Michalak, A. σ-Donor and π-Acceptor Properties of Phosphorus Ligands: An Insight from the Natural Orbitals for Chemical Valence. *Inorg. Chem.* **2010**, *49*, 578–582. [CrossRef] [PubMed]

82. Mata, I.; Alkorta, I.; Molins, E.; Espinosa, E. Universal Features of the Electron Density Distribution in Hydrogen-Bonding Regions: A Comprehensive Study Involving H···X (X=H, C, N, O, F, S, Cl, π) Interactions. *Chem. Eur. J.* **2010**, *16*, 2442–2452. [CrossRef] [PubMed]
83. Alkorta, I.; Solimannejad, M.; Provasi, P.; Elguero, J. Theoretical Study of Complexes and Fluoride Cation Transfer between N2F+ and Electron Donors. *J. Phys. Chem. A* **2007**, *111*, 7154–7161. [CrossRef] [PubMed]
84. Cremer, D.; Kraka, E. A description of the chemical bond in terms of local properties of electron density and energy. *Croat. Chem. Acta* **1984**, *57*, 1259–1281.
85. Rozas, I.; Alkorta, I.; Elguero, J. Behavior of ylides containing N, O, and C atoms as hydrogen bond accepters. *J. Am. Chem. Soc.* **2000**, *122*, 11154–11161. [CrossRef]
86. Poater, J.; Solà, M.; Viglione, R.G.; Zanasi, R. Local Aromaticity of the Six-Membered Rings in Pyracylene. A Difficult Case for the NICS Indicator of Aromaticity. *J. Org. Chem.* **2004**, *69*, 7537–7542. [CrossRef]
87. Poater, J.; Bofill, J.M.; Alemany, P.; Solà, M. Role of Electron Density and Magnetic Couplings on the Nucleus-Independent Chemical Shift (NICS) Profiles of [2.2]Paracyclophane and Related Species. *J. Org. Chem.* **2006**, *71*, 1700–1702. [CrossRef]
88. Sánchez-Sanz, G. Aromatic behaviour of benzene and naphthalene upon pnicogen substitution. *Tetrahedron* **2015**, *71*, 826–839. [CrossRef]
89. Sánchez-Sanz, G.; Trujillo, C.; Rozas, I.; Alkorta, I. Influence of fluoro and cyano substituents in the aromatic and antiaromatic characteristics of cyclooctatetraene. *Phys. Chem. Chem. Phys.* **2015**, *17*, 14961–14971. [CrossRef]
90. Trujillo, C.; Sánchez-Sanz, G. A Study of π–π Stacking Interactions and Aromaticity in Polycyclic Aromatic Hydrocarbon/Nucleobase Complexes. *ChemPhysChem* **2016**, *17*, 395–405. [CrossRef]
91. Sánchez-Sanz, G.; Alkorta, I.; Trujillo, C.; Elguero, J. A theoretical NMR study of the structure of benzynes and some of their carbocyclic and heterocyclic analogs. *Tetrahedron* **2012**, *68*, 6548–6556. [CrossRef]
92. Kusakiewicz-Dawid, A.; Porada, M.; Dziuk, B.; Siodlak, D. Annular Tautomerism of 3(5)-Disubstituted-1H-pyrazoles with Ester and Amide Groups. *Molecules* **2019**, *24*, 2632. [CrossRef] [PubMed]